

¹ Confirmation of Mg/Ca ratios as palaeothermometers in Atlantic limpet
² shells

³ Niklas Hausmann^{a,*}, Donna Surge^b, Ivan Briz i Godino^c

^aLeibniz Zentrum für Archäologie, Ludwig-Lindenschmit-Forum 1, Mainz, Germany, 55116

^bUniversity of North Carolina, 104 South Road, 225 Geology Building, Chapel Hill, NC, US, 27599-3315

^cDepartment of Evolutionary Biology, Ecology and Environmental Science, Biodiversity Research Institute (IRBio), University of Barcelona, Avinguda Diagonal, 643, Barcelona, Spain, 8028

⁴ **Abstract**

This study provides a reassessment of Magnesium to Calcium (Mg/Ca) ratios in Atlantic limpet shells to determine past sea surface temperatures (SST). While *Patella depressa* along the Spanish shoreline has repeatedly produced reliable correlations between SST and Mg/Ca ratios, this relationship is not the case for other patelloid species. *Patella vulgata*, *Nacella deaurata*, and *N. magellanica* have been studied using Mg/Ca ratios with mixed or contrary results. In this study, we present elemental maps of these three species together with oxygen isotope ratios ($\delta^{18}\text{O}$) that confirm a good relationship with SST. Our dataset also reassesses a specimen which was previously unsuccessful in providing significant correlations between $\delta^{18}\text{O}$ values and Mg/Ca ratios. By reassessing these species and including modern and archaeological specimens (n=12) from three patelloid species (*P. vulgata*, *N. deaurata*, and *N. magellanica*) we further add to the growing set of evidence for the reliable use of Mg/Ca ratios to detect palaeotemperature change. As a result, these species can in the future serve to determine ontogenetic age and season of capture as well as to reveal locations of interest within the growth record (i.e. annual temperature minima and maxima) for the targeted analysis using $\delta^{18}\text{O}$ and clumped isotope analysis.

⁵ **Keywords:** Sclerochronology, Patella, Nacella, LIBS, Mg/Ca

⁶ **1. Introduction**

Limpet shells are commonly found within archaeological sites and past shorelines due to their robust carbonate structure and the long-term use of limpets as a marine food source (Álvarez et al., 2011, Robson et al. (2023)). They have been successfully studied in the context of coastal subsistence economies and site occupation on seasonal (Shackleton, 1973; ?; Bosch et al., 2018) or long-term scales (Ortiz et al., 2015), as well as archives of palaeotemperature (Fenger et al., 2007; Surge and Barrett, 2012; Wang et al., 2012; Colonese et al., 2012; Ferguson et al., 2011). Determining past sea surface temperature (SST) change recorded in patelloid limpet shells largely relies on the measurement of $\delta^{18}\text{O}$ values within the calcitic parts of the shell, but attempts have been made to also use elemental ratios, such as magnesium to calcium (Mg/Ca) ratios (Graniero et al., 2017; Ferguson et al., 2011), to have an alternative measure that potentially provides a more accurate SST estimate than $\delta^{18}\text{O}$ -values, as the latter proxy is affected by changes in the mixing of fresh- and saltwater. In addition, the data acquisition of elemental ratios — either through laser-ablation-isotope-ratio-mass-spectrometry (LA-ICP-MS) or laser induced breakdown spectroscopy (LIBS), can be

*Corresponding author

Email address: niklas@palaeo.eu (Niklas Hausmann)

19 much faster and cost-effective, increasing the number of specimens that can be studied overall (Durham
20 et al., 2017; Hausmann et al., 2023).

21 Problematically, links between Mg/Ca ratios and SST changes in many marine mollusc shells, including
22 limpets, have shown to be unreliable (Surge and Lohmann, 2008; Wanamaker et al., 2008; Schöne et al., 2010;
23 Freitas et al., 2012; Graniero et al., 2017; Poulain et al., 2015; Vihtakari et al., 2017). This is particularly
24 the case where there is little available additional information on metabolic processes, organic components of
25 the shell matrix, intra-increment and intra-shell variability, and growth rates, which can independently and
26 unpredictably affect Mg/Ca ratios and confound their interpretation as a temperature proxy. Confusingly,
27 in some cases multiple different temperature equations have been found for the same species (see Freitas *et*
28 *al.* (2012) and Vihtakari *et al.* (2017) and references therein). Coeval specimens sharing one locality can
29 also show differences in their relation to SST (Hausmann et al., 2019). Where the use of Mg/Ca ratios as
30 a palaeotemperature proxy was successful, anomalous patterns in some specimens had to be filtered out by
31 hand, reducing the overall robustness of the results of those successful studies (Ferguson et al., 2011).

32 Recent research particularly of *Patella* spp. in the Mediterranean and southwest Europe have provided
33 promising results (Hausmann et al., 2019; García-Escárzaga et al., 2015, 2018). However, there remains a
34 lack of clarity for Atlantic limpet species, particularly since it was shown, that the Mg/Ca ratio in their
35 shells are not reliable recorders of palaeotemperature (Graniero et al., 2017).

36 In this study we will repeat and expand the analysis of Atlantic limpets to determine the reliability of
37 Mg/Ca ratios as palaeotemperature proxies. To do this, we sampled a set of previously published and
38 unpublished limpet specimens dating to modern and archaeological contexts using LIBS. LIBS allows us to
39 carry out 2D imaging of entire shell sections, which allows navigation of the complex elemental structure of
40 the shell and better separate the external, temperature-related changes from the internal and less understood
41 factors that influence the Mg/Ca ratio. By working with already published datasets, we were able to
42 simultaneously avoid costs for new high-resolution $\delta^{18}\text{O}$ -data, to use real-world examples, and to also provide
43 pilot-data for areas of existing research interest. Generally establishing the usefulness and reliability of
44 Mg/Ca ratios as SST proxy in limpets provides a platform for future research and an important steppingstone
45 to a better understanding of elemental ratios in other marine mollusc shells.

46 2. Materials and Methods

47 2.1. Limpet specimens

48 The analysed specimens, their origin and respective studies with research background information can be
49 found in Table 1. Here we will briefly summarise their contextual information, which can be accessed in
50 more detail at the respective studies (Nicastro et al., 2020; Surge and Barrett, 2012; Graniero et al., 2017).
51 While those studies also included other specimens, their accessibility or state of preservation did not allow
52 them to be re-analysed.

Table 1: Overview of the modern and archaeological limpet specimens analysed in this study.

Context	Study	Species	Location	Sample ID	Previous analyses
Modern	(Nicastro et al., 2020)	<i>N. deaurata</i>	Cambaceres Bay - Tierra del Fuego (AR)	ND-1016-3 ND-1016-4 NM-1016-1 NM-1016-3	$\delta^{18}\text{O}$ and $\delta^{13}\text{C}$ analysis
		<i>N. magellanica</i>			
	(Graniero et al., 2017)	<i>P. vulgata</i>	Rack Wick Bay - Westray (UK)	ORK-LT5	$\delta^{18}\text{O}$ and $\delta^{13}\text{C}$ analysis; Mg, Li, Sr, Ca.
		<i>P. vulgata</i>	Rack Wick Bay - Westray (UK)	QG1-7188-1 QG1-7189-2	$\delta^{18}\text{O}$ and $\delta^{13}\text{C}$ analysis
Archaeological	(Surge and Barrett, 2012)				

Context	Study	Species	Location	Sample ID	Previous analyses
				QG2-1061-1	
				QG2-1064-1	
				QG2-7180-1	
				QG2-7180-2	
				QG1-7246-1	

53 Specimens were sourced from two main locations: the Beagle Channel in Tierra del Fuego (Argentina)
 54 and the island of West Ray in the Orkney archipelago of Scotland (UK). Four modern specimens were
 55 collected from the Beagle Channel in Cambaceres Bay in October 2016. The area receives around 570 mm
 56 of precipitation, but the channel waters are predominantly influenced by marine currents and in the period
 57 of October 2015 to October 2016 stayed around 30.7 ± 0.7 psu (practical salinity units) (Nicastro et al.,
 58 2020). SSTs range from 4.7°C in August to 10°C in February (Figure 1 – red line).

59 On Westray one modern shell (ORK-LT5) was collected in Rack Wick Bay in August 2009 and has been
 60 previously analysed for $\delta^{18}\text{O}$ and $\delta^{13}\text{C}$ values, as well as LA-ICP-MS (Graniero et al., 2017). Westray lies
 61 about 70 km north of the Scottish mainland and experiences virtually no freshwater input with salinity
 62 values of 34.0 – 34.5 psu (Inall et al., 2009). The annual SST ranges from 6.3°C in March to 13.8°C in
 63 August (Figure 1 – blue line).

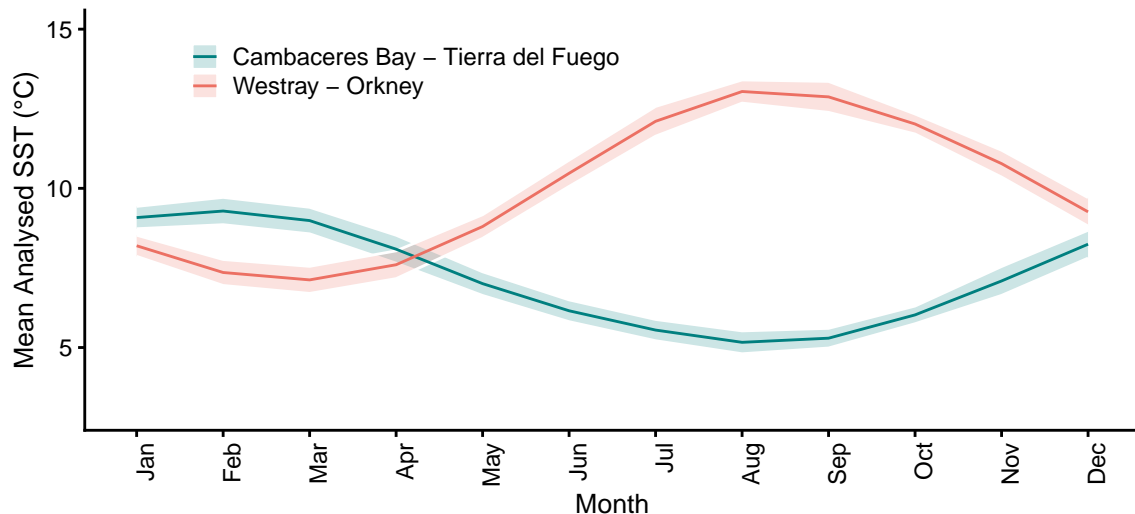


Figure 1: Monthly Sea Surface Temperature values averaged from years. SST values were sourced from Good et al. (2020).

64 We also studied 7 archaeological specimens of *P. vulgata* from the Quoygrew site on Westray dating to 900
 65 – 1200 CE. These shells have previously been studied to characterise seasonal temperature change during
 66 the Medieval Climate Anomaly (810 – 1229 CE) (Surge and Barrett, 2012). Together they show a range of
 67 lifespans, with some comparatively long lived for their size (QG1-7246-1, 12 years within 16 mm of growth)
 68 making them particularly susceptible to within-shell time-averaging because of slow growth rates. That said,
 69 the majority are under 5 years old yielding sufficiently fast growth to nearly capture seasonal amplitudes of
 70 SST.

71 2.2. Methods

72 2.2.1. Mg/Ca ratios

73 Mg/Ca elemental imaging was carried out using LIBS at the Leibniz Zentrum für Archäologie (Mainz-
74 Germany) following previously published methods (Hausmann et al., 2023). The imaging involves the
75 ablation of the shell section using an infrared (1064 nm) laser (1–2 mJ, 100 Hz) onto a surface area of 20–30
76 μm to generate a plasma plume. This plume emits light, which is measured using a synchronised spectrometer
77 (delay time = 0.5 μs , integration time = 1 μs). The resulting light spectrum quantifies the emission lines of
78 Magnesium (MgII; 279.553 nm) and Calcium (CaII; 315.887 nm) to determine their intensity ratio. While
79 these two peaks alone do not represent the molar concentrations of both elements (as opposed to calibration
80 free LIBS; e.g. (?)), the intensity ratio is linearly correlated to the molar concentration (Hausmann et al.,
81 2017) and can be used as a reliable indicator of Mg/Ca variation within the shell carbonate. All values
82 reported here are in arbitrary units based on the ratio of intensities of the peaks above.

83 Using this system we carried out elemental imaging of the shell specimens at a resolution of 50–100 μm
84 distance between sampling spots. Each spot was irradiated 10 times with the first 3 spectra discarded as a
85 cleaning step and the remaining spectra summed to get an average Mg/Ca intensity ratio for each sample
86 spot. Subsequently, we re-sampled the section using a line scan at 10 μm resolution. This leads to an overlap
87 between sample spots, but also allows for a continuous record without gaps. Intensity ratios were filtered
88 for cases with high relative standard deviation (i.e., more than 10%). These occurred in places where the
89 previous sampling procedures for carbonate powder as part of the oxygen isotope analysis left an uneven
90 sample surface introducing variability in the plasma generation and thus uncertainty in the data of these
91 locations.

92 2.2.2. Oxygen isotope ratios

93 High-quality $\delta^{18}\text{O}$ values were acquired from previous publications on *P. vulgata* (Surge and Barrett, 2012;
94 Graniero et al., 2017), *N. deaurata* and *N. magellanica* (Nicastro et al., 2020), in which detailed descriptions
95 of the methodology for the stable isotope analyses can be found. In short, all shells were sectioned along the
96 maximum growth axis to expose the internal growth structure. From the exposed section carbonate powder
97 samples were acquired using a micromill with resolutions of 100–200 μm and by targeting the calcitic M+2
98 layer of the shells. Analytical precision of the isotope ratios was consistently at 0.05–0.10‰ and values are
99 reported in per mil units (‰) relative to the VPDB (Vienna Pee Dee Belemnite) standard.

100 Figure 2 and Figure 3 show the previously acquired sequential $\delta^{18}\text{O}$ -values of limpet shells by species
101 (*Nacella* spp., and *Patella vulgata*, respectively). Due to the high-resolution sampling, all shells show
102 seasonally resolved and multi-year quasi-sinusoidal records of SST change, with *Nacella* spp. shells living
103 2–3 years and *P. vulgata* living regularly over 3 years. In those instances where longer lifespans resulted in
104 slow growth rates below 1 mm/yr (i.e. specimen QG1-7246-1, Figure 3 b), the temporal-resolution is reduced
105 from more than a dozen of samples per year, to only around 7.

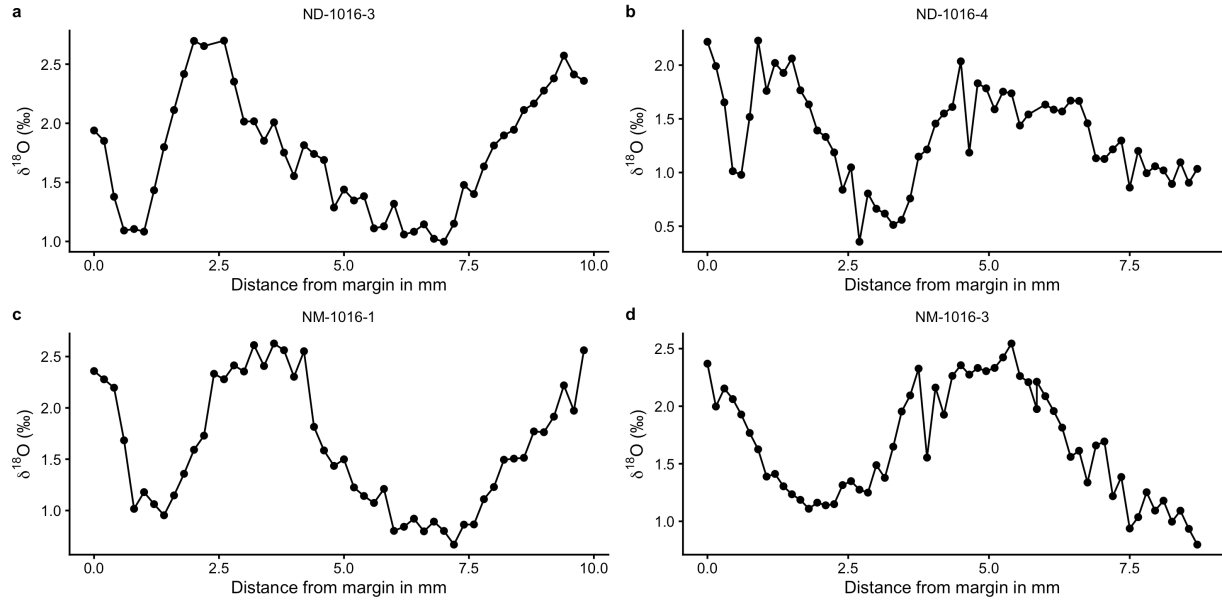
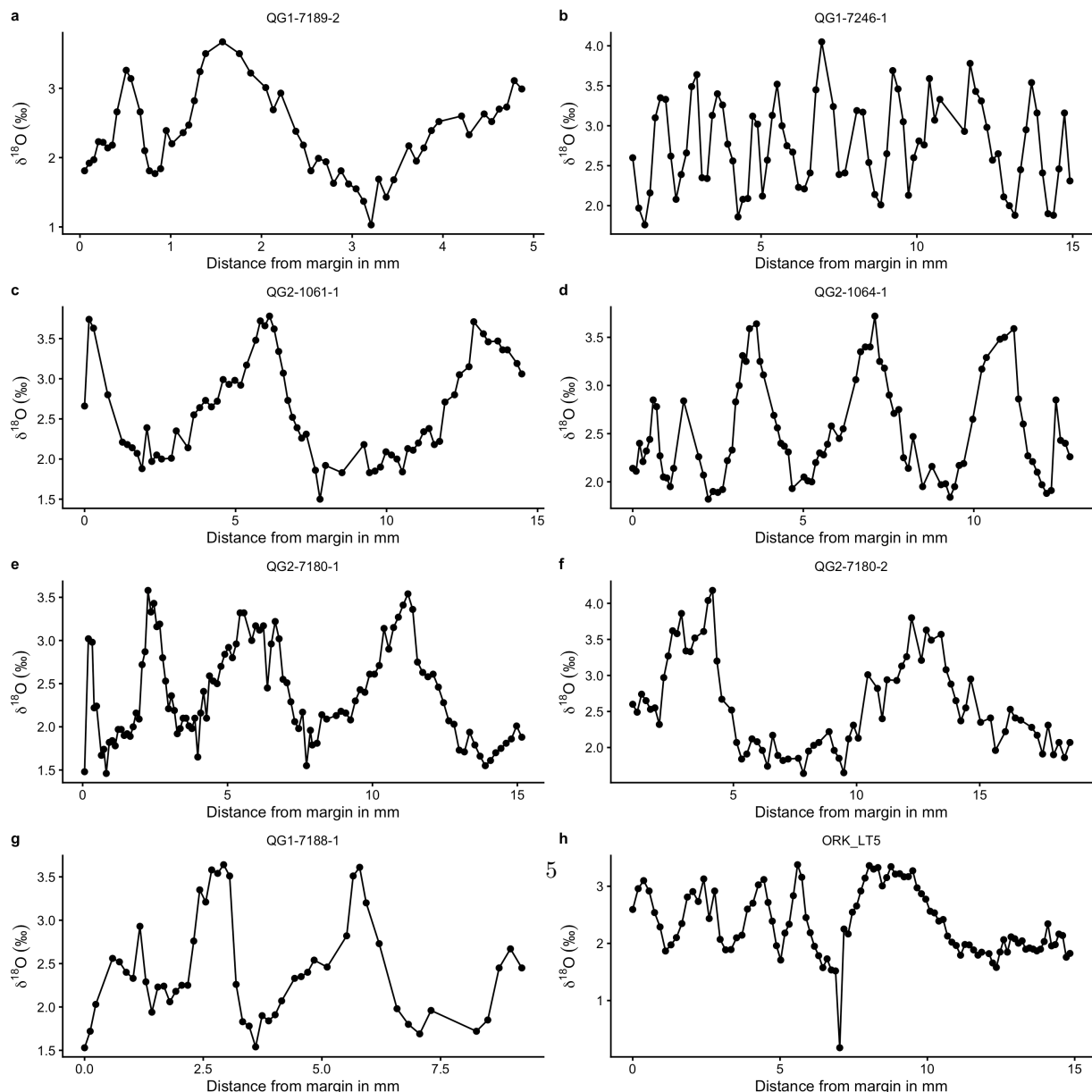


Figure 2: Isotope values of *Nacella* spp. limpet shells from Cambaceres Bay.



106 2.3. Dynamic Time Warping

107 Because it is not possible to directly associate the exact sample locations used in the analysis of oxygen
108 isotope ratios with the LIBS data, we used dynamic time warping (DTW) to align the time series of $\delta^{18}\text{O}$
109 values and Mg/Ca ratios. DTW is an algorithm that measures similarity between two proxy sequences,
110 which may vary in sampling resolution or interval. By stretching or compressing sections of the series, DTW
111 finds the probable alignment between the two sequences. This allows us to compare the proxy datasets
112 more effectively, ensuring that the temporal dynamics of each shell are accurately matched despite possible
113 discrepancies in sampling intervals or rates. We applied the DTW algorithm using the `dtw` package in R
114 ([Giorgino, 2009](#); [R Core Team, 2020](#)), which provides a robust framework for aligning time series data. This
115 involved selecting appropriate distance measures and constraints to ensure meaningful alignment (see code
116 in (?)). The process involved iterative adjustments to minimise the overall distance between corresponding
117 points in the two data sets.

118 **3. Results**

119 3.1. *Patella vulgata*

120 The elemental imaging of *P. vulgata* shells consistently showed repeating patterns of Mg/Ca intensity ratio
121 changes with high Mg/Ca intensity ratios indicating high temperature periods and low ratios indicating
122 low temperature periods. As examples, Figure 4 shows the 2D-distribution of elemental ratios across the
123 entire section of ORK-LT5 and the preserved anterior side of QG1-7188-1 (additional maps can be found
124 in the supplementaries). The repeating patterns are found across the calcitic layers that are exterior to the
125 myostracum (layers m+2 and m+3) as well as the layers that are interior (m-2)(see Fenger et al. ([2007](#))
126 for a detailed explanations of microstructural layers in *P. vulgata*). The layer m-1, which is also interior,
127 consists of aragonite and is seen in Figure 4 in grey, as its Mg/Ca intensity ratio consistently falls below
128 the range of interest (0.2 and above). Compared to other patelloid shells, some of whose interior is almost
129 entirely made of aragonite, this layer is very thin.
130

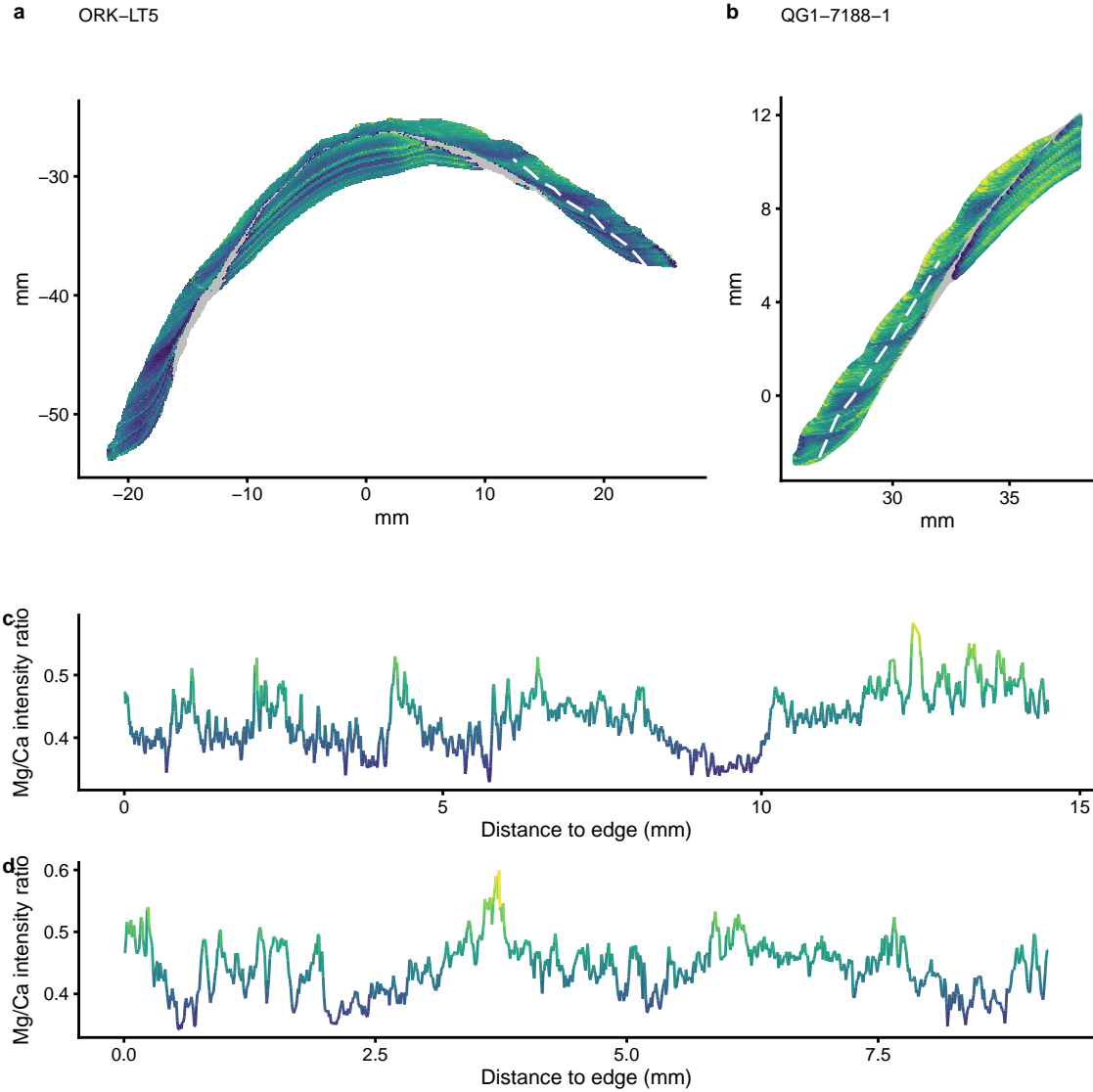


Figure 4: Example LIBS maps and line scans of analysed specimens. (a+c) ORK-LT and (b+d) QG1-7188-1. Note that the ranges of Mg/Ca intensity ratios are not identical but are chosen arbitrarily to increase contrast. Areas in grey consist of low-Mg aragonite and fall outside the chosen colour-range.

Both specimens in Figure 4 show increased Mg/Ca intensity ratios towards the outside of the shell and some degree of intra-increment variability. This is particularly visible in Figure 4 b, where Mg/Ca intensity ratios range from ~0.5–0.7 in the first year of growth (9–12 mm on the y-axis). A similar pattern is visible in the interior m-2 layer of ORK-LT5 (Figure 4 a), which increase towards the anterior of the shell (0–10 mm on the x-axis).

Line scans also indicate well the quasi-sinusoidal change of Mg/Ca intensity ratios expected based on the stable isotope data and elemental imaging. That said, some of the variability of Mg/Ca intensity ratios within one season such as the summer period of QG1-7188-1 between 0.5 and 2.0 mm distance to the shell edge (Figure 4 d), is visible in a more dramatic manner than it appears in the 2D image. This shows the downside of line-scanning as opposed to the broader milling approach used for the analysis of carbonate

¹⁴¹ powder (Ferguson et al., 2011).

¹⁴² Figure 5 shows the line scan of ORK-LT5 in comparison to its $\delta^{18}\text{O}$ values (similar graphs for other
¹⁴³ specimens can be found in the supplementaries). The measurements of the distance to the shell edge are
¹⁴⁴ not entirely identical, most likely because one growth increment can have a range of distances to the edge,
¹⁴⁵ depending on where one measures, and a line scan along the interior would be shorter than a line scan along
¹⁴⁶ the exterior. That said, increases and decreases of both proxies seem to mirror each other and to be well
¹⁴⁷ aligned.

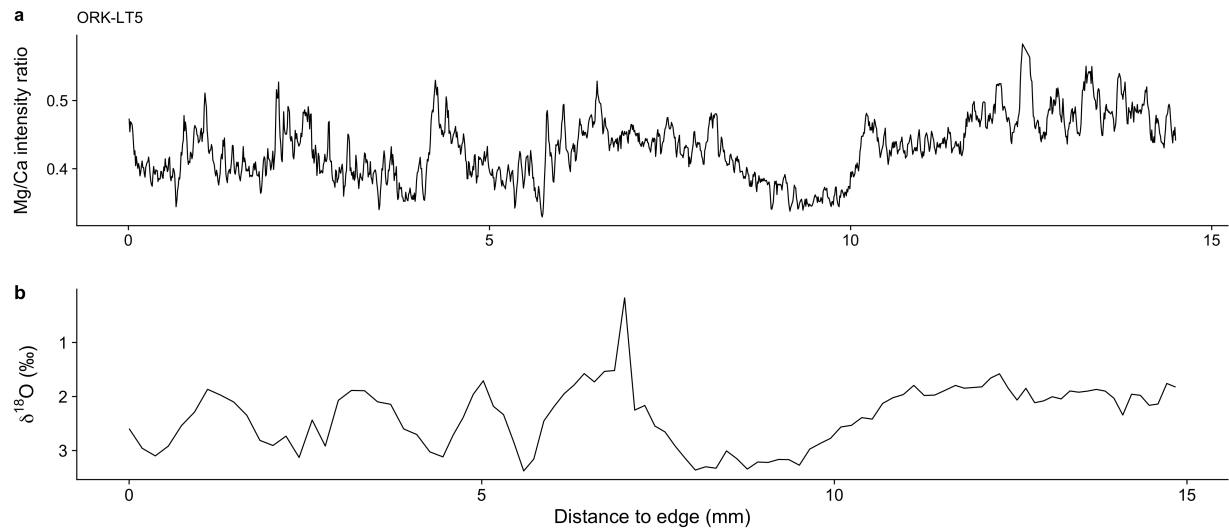


Figure 5: Comparison of LIBS line-scan and sequential $\delta^{18}\text{O}$ -values of specimen ORK-LT5

¹⁴⁸ Aligning the records programmatically using dynamic time warping, allowed us to compare both proxies
¹⁴⁹ for each specimen directly to determine specimen-specific equations and quantify the correlation of both
¹⁵⁰ proxies (Figure 6). The equations for all specimens are different but the majority (barring one: QG1-7246-
¹⁵¹ 1) do seem to cluster around shared parameters ($\delta^{18}\text{O} = 0.6 - 0.065 * \text{Mg/Ca}$). The various coefficients of
¹⁵² determination (R^2) range between 0.81 (QG1-7246-1) and 0.95 (QG1-7189-2). These specimens are also the
¹⁵³ oldest and youngest specimens, respectively, suggesting that lower growth rates and time averaging had a
¹⁵⁴ negative effect on the correlation of both proxies. The mean R^2 value of the individual *P. vulgata* specimens
¹⁵⁵ is 0.89, suggesting a generally good fit between the two proxies.

¹⁵⁶ 3.2. *Nacella spp.*

¹⁵⁷ The LIBS data for *Nacella spp.* specimens is less straightforward with shells being much thinner than
¹⁵⁸ *P. vulgata* and thus patterns being more difficult to discern. Both specimens (ND-1016-3 and NM-1016-3)
¹⁵⁹ shown as examples in Figure 7 (see additional graphs in supplementaries) also experience increases of Mg/Ca
¹⁶⁰ intensity ratio towards the exterior of the shell, similar to the *P. vulgata* specimens from Orkney. This intra-
¹⁶¹ increment heterogeneity combined with the thinness of the shell, further complicates their analysis compared
¹⁶² to *P. vulgata* or other *Patella* species (Hausmann et al., 2019). Nevertheless, repeating patterns were visible
¹⁶³ in the anterior section of the shell, which were also mirrored in the inner layers (m-2) of specimens NM-1016-3
¹⁶⁴ (Figure 7 b).

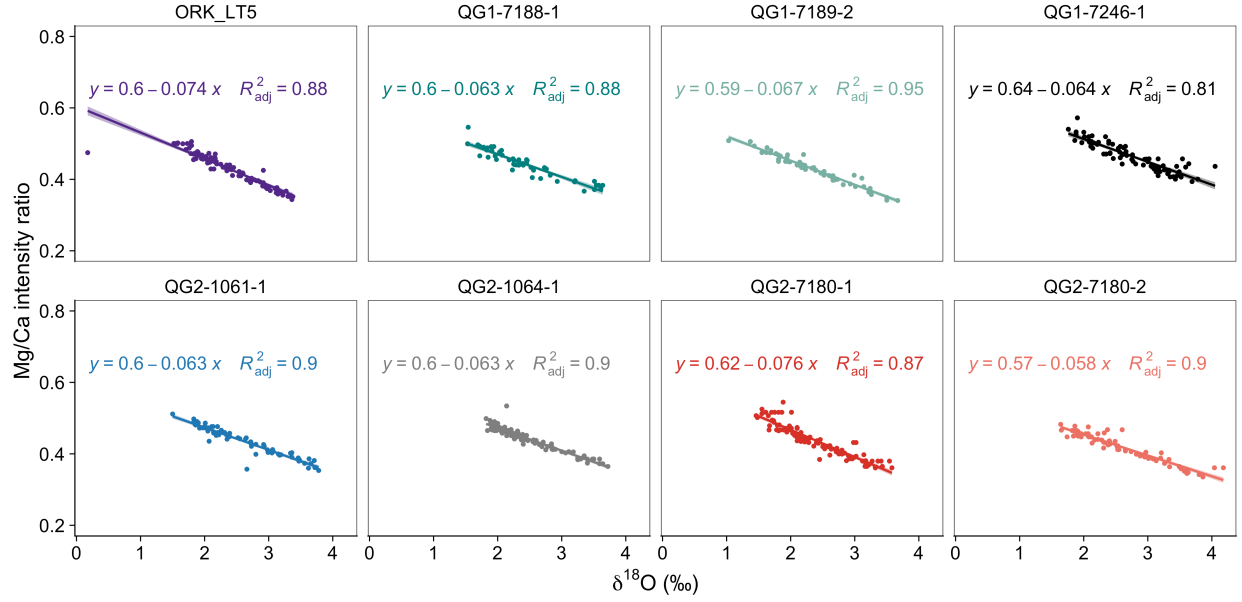


Figure 6: Correlation graphs for *Patella vulgata* specimens.

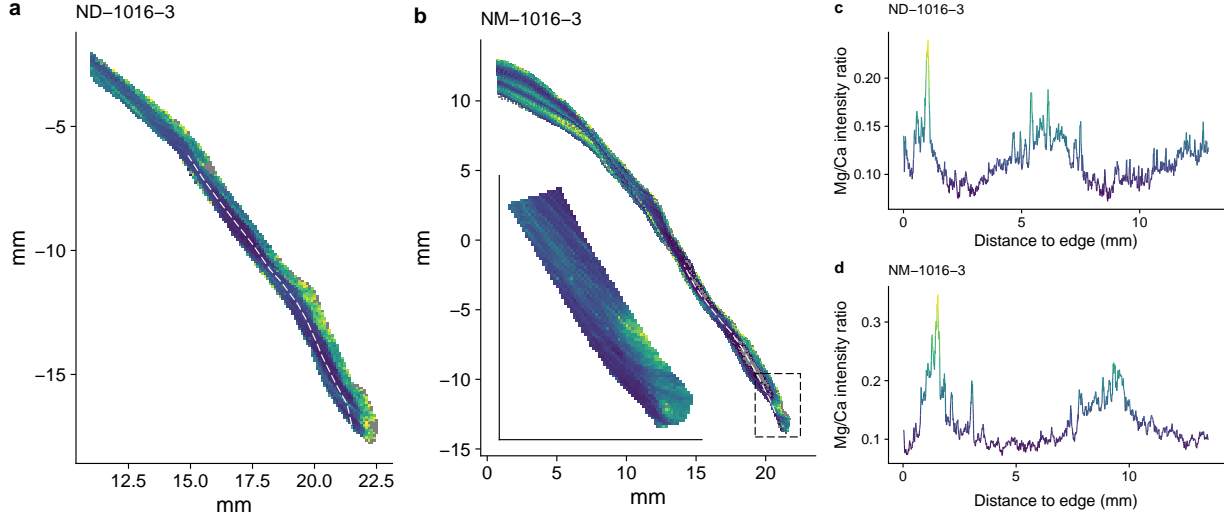


Figure 7: Example LIBS maps and line scans of analysed *Nacella* spp. specimens. (a+c) ND-1016-3 and (b+d) NM-1016-3. Note that the ranges of Mg/Ca intensity ratios are not identical but are chosen arbitrarily to increase contrast. Areas in grey consist of low-Mg aragonite and fall outside the chosen colour-range. Note the inset in (c) where the shell edge has been resampled using a higher resolution (50 µm instead of 100 µm) to better understand the Mg/Ca ratios at the shell edge.

165 Interestingly, the Mg/Ca intensity ratios in the *Nacella* spp. shells were much lower (0.05–0.30) than those
 166 seen in other patelloid species (e.g. 0.3–0.7 in *P. vulgata* above, or 0.5–1.5 in Hausmann *et al.* (2023))
 167 using the same emission lines. While the intensity ratio depends chiefly on the chosen emission lines to
 168 calculate the proportion of the chosen Magnesium to the chosen Calcium peak, the low ratios still indicate
 169 lower concentrations than seen elsewhere or seen only in aragonitic parts of e.g. *Patella* shells. Similar
 170 observations have been made before (Graniero *et al.*, 2017). Strong intra-increment heterogeneities are

visible along the exterior of the shells ($m+3$ layer), where Mg/Ca intensity ratios are higher, particularly in specimen ND-1016-3 (Figure 7). The step from lower to higher along the increment is not gradual, as is the case in NM-1016-3 (see inset of Figure 7 b), but rather stepwise. Sampling across this boundary in a linear scan would most likely lead to erroneous results. Also sampling across gradual changes as in NM-1016-3 can influence the overall correlation graph for a specimen.

Line scans reflect well the changes previously indicated by $\delta^{18}\text{O}$ values and also indicate about two years of recorded growth. That said, the 2D imaging suggests that in both specimens a third summer can be added to the total record, which is not captured by the line scans.

Figure 8 shows the line scans of ND-1016-3 and NM-1016-3 in comparison to their $\delta^{18}\text{O}$ values (similar graphs for the other *Nacella* spp. specimens can be found in the supplementaries). Compared to the *P. vulgata* records, these mirror each other much more clearly, due to the brief period recorded in the shells and thus a lower chance of misaligning annual extremes.

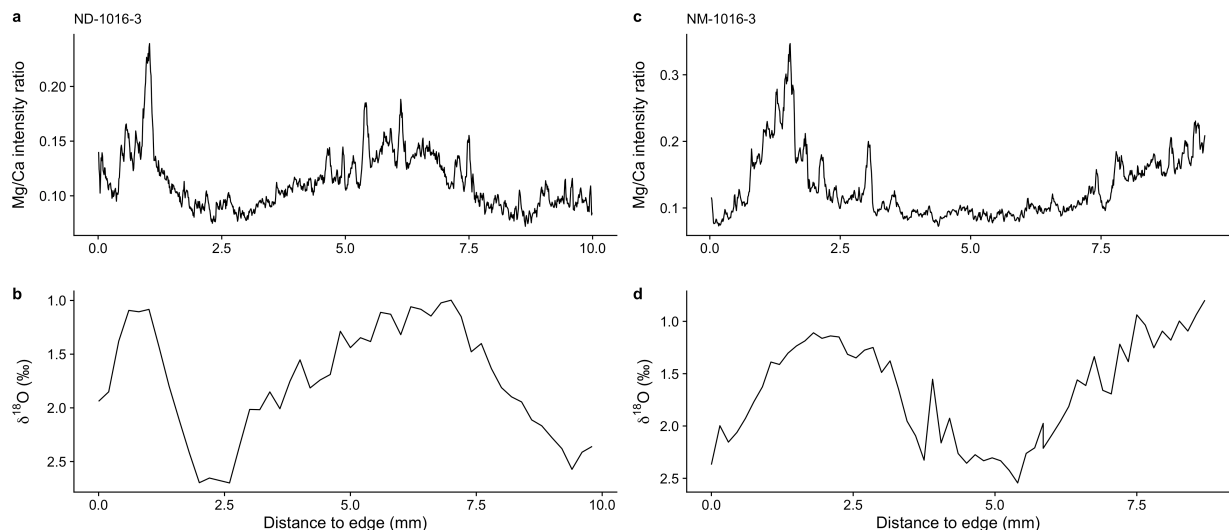


Figure 8: Comparison of LIBS line-scan and sequential $\delta^{18}\text{O}$ -values of *Nacella* spp. specimens.

The *Nacella* spp. specimens showed similarly clustered correlations, which interestingly were not grouped by species. In fact, specimens ND-1016-3 (*Nacella deaurata*) and NM-1016-3 (*N. magellanica*) are almost identical in their fitted equations (Figure 9). Both also share a high coefficient of determination (R^2) of 0.95 and 0.92 respectively, with the remaining specimens being somewhat lower ($R^2 = 0.76$ for ND-1016-4 and $R^2=0.84$ for NM-1016-3). The mean R^2 value for each *N.* species is 0.86 for *N. deaurata* and 0.88 for *N. magellanica*. Why two specimens of different species are so well aligned is not entirely certain and randomness cannot for now be ruled out. That said, since they both have a high R^2 value, it might just be that they were both minimally affected by factors other than SST, including the sampling location of our line scans.

4. Discussion

The Mg/Ca ratios from the 2D elemental imaging present positive results suggesting that SST is the main factor influencing variations in Mg/Ca ratios in three Atlantic limpet species. Annually repeating patterns of increasing (spring/summer) and decreasing (autumn/winter) SST were also visible in the line scans, albeit less straightforward than in the 2D-data. Nevertheless, the resulting R^2 -values for each species were high (*P. vulgata* mean $R^2=0.89$, *N. deaurata* mean $R^2=0.86$, *N. magellanica* mean $R^2=0.88$). These results are

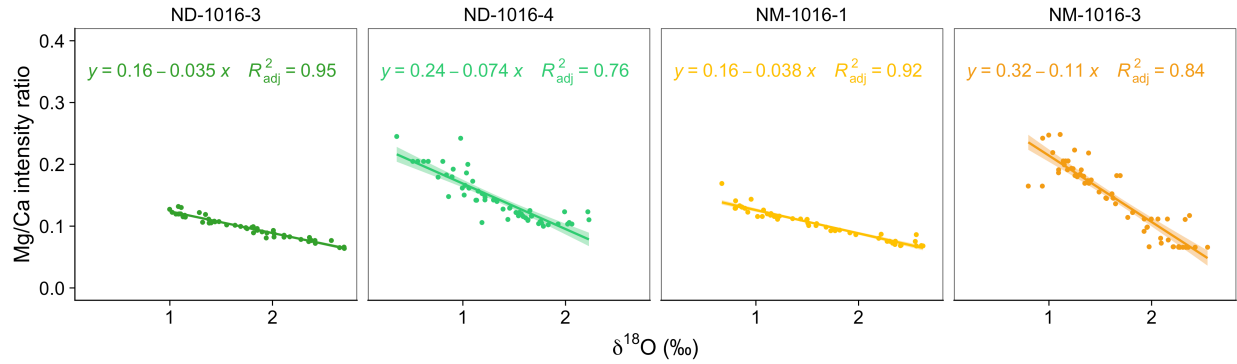


Figure 9: Correlation graphs for *Nacella* spp. specimens

similar to previously published data on other *Patella* species shells (Table 2): R^2 values of *P. depressa* lie between 0.78 and 0.87 (García-Escárzaga et al., 2021), for *P. caerulea* from the Mediterranean between 0.78 and 0.96 — barring one outlier of 0.33 (specimen MP64A), which had increased Mg/Ca ratios in increments with rich organic contents (Hausmann et al., 2019).

Table 2: Correlations of Mg/Ca ratios with $\delta^{18}\text{O}$ values and SST found in other studies. Bold R^2 values are interpreted as outliers. * indicates that only SST data and no other geochemical data was used. ** these samples were used to determine a shared R^2 -value of 0.79.

Species	Locality	Specimen	R^2	Study
<i>P. depressa</i>	Northern Spain	LAN541	0.87	(García-Escárzaga et al., 2021)
		LAN545	0.86	
		LAN554	0.78	
		LAN559	0.82	
<i>P. caerulea</i>	Croatia	ISTPC1	0.9	(Hausmann et al., 2019)
		ISTPC2	0.84	
	Crete	AF1911A	0.91	
		AF3003A	0.92	
	Israel	AKKPC2	0.96	
		AKKPC3	0.89	
		FRMPC1	0.84	
		FRMPC2	0.96	
	Libya	MO31A	0.83	
		MP64A	0.33	
		MP67A	0.96	
		MP68A	0.81	
<i>P. rustica</i>	Malta	MA10	0.82	(Ferguson et al., 2011)
		TUNPC1	0.81	
	Tunisia	TUNPC2	0.78	
		ANTPC1	0.95	
	Turkey	ANTPC2	0.93	
		KIZPC1	0.94	
		KIZPC2	0.86	
	Gibraltar	JL1	0.02	
<i>P. caerulea</i>	Gibraltar	JL2	0.8**	
		JM00	0.69**	
		JM30	0.83**	
<i>P. vulgata</i>	Orkney	ORK-LT5	not reported, here 0.88	(Graniero et al., 2017) and this study

P. rustica has two studied specimens (JL1 and JL2) with R^2 -values of 0.02 and 0.80, respectively (Ferguson et al., 2011) (Figure 10). Together with the data from two *P. caerulea* shells (JM00 and JM30 with R^2 -values

of 0.69 and 0.83), the data from JL2 was used to determine a general Mg/Ca-SST relationship with an R^2 value of 0.79. JL1 was disregarded in that calculation, as well as the second year of growth in JM00, which produced anomalous data. While no additional information about those specimens is available, it seems likely that the discarded Mg/Ca ratios from JM00, which were interpreted as an ontogenetic trend, were potentially influenced by the same intra-increment heterogeneity we see in some of our shell specimens as well. Since these shells were analysed by homogenising the carbonate powder of the m+2 layer and the more exterior m+3 layer, these heterogeneities could have potentially increased the Mg/Ca ratio unpredictably, leading to what might look like an ontogenetic trend in a linear dataset. Whether these anomalies affected JL1 in the same way, albeit stronger, is not clear but it might well be possible.

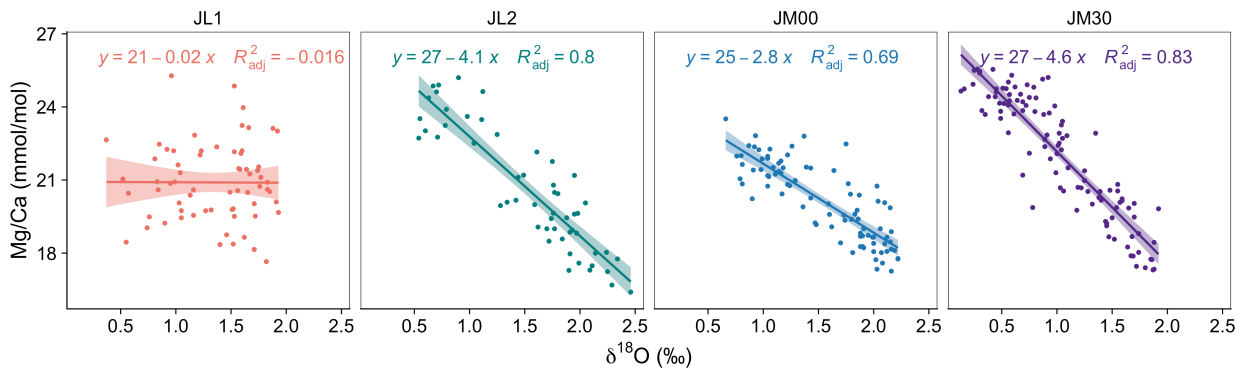


Figure 10: Correlation graphs for Ferguson et al., (2011) specimens.

Another shell whose results we aim to explain further is ORK-LT5 (Figure 4), which has previously been shown to have no substantial correlation with $\delta^{18}\text{O}$ values or SST by implication (Graniero et al., 2017). In contrast to other specimens in this study, we were able to resample this specimen and acquire Mg/Ca data on a slightly higher resolution (20–30 μm spots in a 100 μm raster compared to 50 μm spots spaced at 150–300 μm) and using 2 dimensions, as well as using a continuous high-resolution line-scan at (20–30 μm spots spaced at 10 μm) (Figure 11). These additional data revealed previously missed summer peaks at around 2–3 mm distance to the shell edge (grey box in Figure 11) and revealed additional growth at the very edge (dashed box in Figure 11) mirroring the change towards warmer temperatures at the time of collection (August). Including these missing parts lead to a better alignment of both records and a resulting R^2 -value of 0.88 (Figure 11).

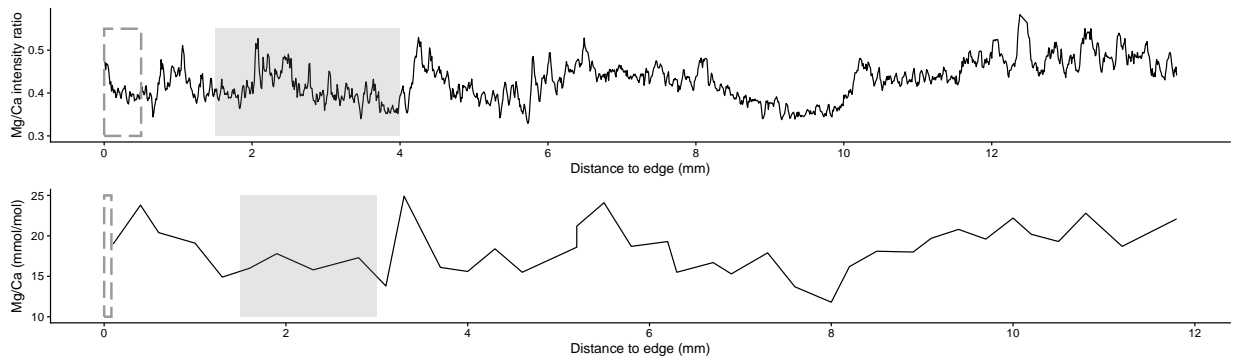


Figure 11: Comparison of previous and new Mg/Ca data for ORK-LT5 explaining the previously unsuccessful correlation of Mg/Ca and $\delta^{18}\text{O}$ -values

We were not able to resample the *Nacella* spp. specimens in Graniero et al. (2017), which had similarly

unrelated records of $\delta^{18}\text{O}$ values and Mg/Ca ratios and pointed to no relationship between elemental ratios and SST at all. However, we were able to source other modern specimens of the same species from Tierra del Fuego, which shall serve here as an indicator. Similar to other patelloid shells, the results of the *Nacella* specimens in our study were successful with high R^2 values (0.76–0.95) and suggest Mg/Ca as a reliable proxy for SST (Figure 8 and supplementaries). Why these results are different from the studied *Nacella* spp. specimens in Graniero *et al.* (2017) is not obvious, but the occasional alignment of the Mg/Ca and $\delta^{18}\text{O}$ records of their shells (Figure 6 in Graniero *et al.* (2017)) indicate that there is some relationship that — potentially due to the low sampling resolution or intra-increment heterogeneity — is not perfectly visible, leading to an overall result of an uncorrelated relationship between Mg/Ca ratios and SST.

5. Conclusion

This study uses LIBS as a novel analytical tool to present high-resolution and 2D information on Mg/Ca concentrations in modern and archaeological patelloid shells and their relationship to sea surface temperature. The results for *P. vulgata*, *N. deaurata*, and *N. magellanica* were consistently promising with mean R^2 values of 0.89, 0.86, and 0.88 respectively.

LIBS elemental imaging provided insight into elemental anomalies found particularly in the external parts (m+3 layer) of the shell, which introduce intra-incremental heterogeneity and which cannot be reconciled with modern SST changes or SST changes recorded in the $\delta^{18}\text{O}$ values of the same shells. Our 2D approach allowed us to avoid these areas of intra-increment heterogeneity and focus on areas that are predominantly controlled by changes in SST.

These results are particularly promising for future analyses of patelloid shells for the study of season of collection in archaeological sites as well as the reconstruction of sub-annual climatic conditions in the past. Shells of the species studied here are widely available along the European Atlantic façade and the Argentinian coastline and make up a significant part of marine mollusc remains in archaeological sites of those regions (Colonese *et al.*, 2011; Villagran *et al.*, 2011; Zangrandino *et al.*, 2016). By using LIBS as a screening tool for targeted $\delta^{18}\text{O}$ analysis, focusing on annual minima and maxima revealed in the Mg/Ca record, researchers can improve cost and time efficiency. This novel method will enable them to increase sample numbers and produce larger, more in-depth climatic studies than previously possible.

6. Acknowledgements

References

- Bosch, M.D., Mannino, M.A., Prendergast, A.L., Wesselingh, F.P., O'Connell, T.C., Hublin, J.J., 2018. Year-round shellfish exploitation in the levant and implications for upper palaeolithic hunter-gatherer subsistence. *J. Archaeol. Sci. Rep.* 21, 1198–1214. doi:[10.1016/j.jasrep.2017.08.014](https://doi.org/10.1016/j.jasrep.2017.08.014).
- Colonese, A.C., Camarós, E., Verdún, E., Estévez, J., Giralt, S., Rejas, M., 2011. Integrated archaeozoological research of shell middens: New insights into hunter-gatherer-fisher coastal exploitation in tierra del fuego. *The Journal of Island and Coastal Archaeology* 6, 235–254. doi:[10.1080/15564894.2011.586088](https://doi.org/10.1080/15564894.2011.586088).
- Colonese, A.C., Verdún-Castelló, E., Álvarez, M., Briz i Godino, I., Zurro, D., Salvatelli, L., 2012. Oxygen isotopic composition of limpet shells from the beagle channel: implications for seasonal studies in shell middens of tierra del fuego. *J. Archaeol. Sci.* 39, 1738–1748. doi:[10.1016/j.jas.2012.01.012](https://doi.org/10.1016/j.jas.2012.01.012).
- Durham, S.R., Gillikin, D.P., Goodwin, D.H., Dietl, G.P., 2017. Rapid determination of oyster lifespans and growth rates using LA-ICP-MS line scans of shell mg/ca ratios. *Palaeogeogr. Palaeoclimatol. Palaeoecol.* 485, 201–209. doi:[10.1016/j.palaeo.2017.06.013](https://doi.org/10.1016/j.palaeo.2017.06.013).
- Fenger, T., Surge, D., Schöne, B., Milner, N., 2007. Sclerochronology and geochemical variation in limpet shells (*Patella vulgata*): A new archive to reconstruct coastal sea surface temperature. *Geochemistry* 8. doi:[10.1029/2006GC001488](https://doi.org/10.1029/2006GC001488).
- Ferguson, J.E., Henderson, G.M., Fa, D.A., Finlayson, J.C., Charnley, N.R., 2011. Increased seasonality in the western mediterranean during the last glacial from limpet shell geochemistry. *Earth Planet. Sci. Lett.* 308, 325–333. doi:[10.1016/j.epsl.2011.05.054](https://doi.org/10.1016/j.epsl.2011.05.054).

- 270 Freitas, P.S., Clarke, L.J., Kennedy, H., Richardson, C.A., 2012. The potential of combined mg/ca and ^{18}O measurements
271 within the shell of the bivalve *pecten maximus* to estimate seawater ^{18}O composition. *Chem. Geol.* 291, 286–293. doi:[10.1016/j.chemgeo.2011.10.023](https://doi.org/10.1016/j.chemgeo.2011.10.023).
- 272 García-Escárzaga, A., Clarke, L.J., Gutiérrez-Zugasti, I., González-Morales, M.R., Martínez, M., López-Higuera, J.M., Cobo,
273 A., 2018. Mg/ca profiles within archaeological mollusc (*patella vulgata*) shells: Laser-induced breakdown spectroscopy
274 compared to inductively coupled plasma-optical emission spectrometry. *Spectrochim. Acta Part B At. Spectrosc.* 148, 8–15.
275 doi:[10.1016/j.sab.2018.05.026](https://doi.org/10.1016/j.sab.2018.05.026).
- 276 García-Escárzaga, A., Martínez-Minchero, M., Cobo, A., Gutiérrez-Zugasti, I., Arrizabalaga, A., Roberts, P., 2021. Using
277 mg/ca ratios from the limpet *patella depressa pennant*, 1777 measured by laser-induced breakdown spectroscopy (LIBS) to
278 reconstruct paleoclimate. *Appl. Sci. (Basel)* 11, 2959. doi:[10.3390/app11072959](https://doi.org/10.3390/app11072959).
- 279 García-Escárzaga, A., Moncayo, S., Gutiérrez-Zugasti, I., González-Morales, M.R., Martín-Chivelet, J., Cáceres, J.O., 2015.
280 Mg/ca ratios measured by laser induced breakdown spectroscopy (LIBS): a new approach to decipher environmental conditions.
281 *J. Anal. At. Spectrom.* 30, 1913–1919. doi:[10.1039/c5ja00168d](https://doi.org/10.1039/c5ja00168d).
- 282 Giorgino, T., 2009. Computing and visualizing dynamic time warping alignments in R: ThedtwPackage. *J. Stat. Softw.* 31,
283 1–24. doi:[10.18637/jss.v031.i07](https://doi.org/10.18637/jss.v031.i07).
- 284 Good, S., Fiedler, E., Mao, C., Martin, M.J., Maycock, A., Reid, R., Roberts-Jones, J., Searle, T., Waters, J., While, J.,
285 Worsfold, M., 2020. The current configuration of the OSTIA system for operational production of foundation sea surface
286 temperature and ice concentration analyses. *Remote Sens. (Basel)* 12, 720. doi:[10.3390/rs12040720](https://doi.org/10.3390/rs12040720).
- 287 Graniero, L.E., Surge, D., Gillikin, D.P., Briz i Godino, I., Álvarez, M., 2017. Assessing elemental ratios as a paleotemperature
288 proxy in the calcite shells of patelloid limpets. *Palaeogeogr. Palaeoclimatol. Palaeoecol.* 465, 376–385. doi:[10.1016/j.palaeo.2016.10.021](https://doi.org/10.1016/j.palaeo.2016.10.021).
- 289 Hausmann, N., Prendergast, A.L., Lemonis, A., Zech, J., Roberts, P., Siozos, P., Anglos, D., 2019. Extensive elemental mapping
290 unlocks mg/ca ratios as climate proxy in seasonal records of mediterranean limpets. *Sci. Rep.* 9, 3698. doi:[10.1038/s41598-019-39959-9](https://doi.org/10.1038/s41598-019-39959-9).
- 291 Hausmann, N., Siozos, P., Lemonis, A., Colonese, A.C., Robson, H.K., Anglos, D., 2017. Elemental mapping of mg/ca
292 intensity ratios in marine mollusc shells using laser-induced breakdown spectroscopy. *J. Anal. At. Spectrom.* 32, 1467–1472.
293 doi:[10.1039/c7ja00131b](https://doi.org/10.1039/c7ja00131b).
- 294 Hausmann, N., Theodoraki, D., Piñon, V., Siozos, P., Lemonis, A., Anglos, D., 2023. Applying laser induced breakdown
295 spectroscopy (LIBS) and elemental imaging on marine shells for archaeological and environmental research. *Sci. Rep.* 13,
296 19812. doi:[10.1038/s41598-023-46453-w](https://doi.org/10.1038/s41598-023-46453-w).
- 297 Inall, M., Gillibrand, P., Griffiths, C., MacDougal, N., Blackwell, K., 2009. On the oceanographic variability of the north-west
298 european shelf to the west of scotland. *J. Mar. Syst.* 77, 210–226. doi:[10.1016/j.jmarsys.2007.12.012](https://doi.org/10.1016/j.jmarsys.2007.12.012).
- 299 Nicastro, A., Surge, D., Briz i Godino, I., Álvarez, M., Schöne, B.R., Bas, M., 2020. High-resolution records of growth
300 temperature and life history of two *nacella* limpet species, tierra del fuego, argentina. *Palaeogeogr. Palaeoclimatol. Palaeoecol.*
301 540, 109526. doi:[10.1016/j.palaeo.2019.109526](https://doi.org/10.1016/j.palaeo.2019.109526).
- 302 Ortiz, J.E., Gutiérrez-Zugasti, I., Torres, T., González-Morales, M., Sánchez-Palencia, Y., 2015. Protein diagenesis in *patella*
303 shells: Implications for amino acid racemisation dating. *Quat. Geochronol.* 27, 105–118. doi:[10.1016/j.quageo.2015.02.008](https://doi.org/10.1016/j.quageo.2015.02.008).
- 304 Poulain, C., Gillikin, D.P., Thébault, J., Munaron, J.M., Bohn, M., Robert, R., Paulet, Y.M., Lorrain, A., 2015. An evaluation
305 of mg/ca, sr/ca, and ba/ca ratios as environmental proxies in aragonite bivalve shells. *Chem. Geol.* 396, 42–50. doi:[10.1016/j.chemgeo.2014.12.019](https://doi.org/10.1016/j.chemgeo.2014.12.019).
- 306 R Core Team, 2020. R core team R: a language and environment for statistical computing. Foundation for Statistical Computing
307 .
- 308 Robson, H.K., Hausmann, N., Milner, N., 2023. Shell middens. Elsevier.
- 309 Schöne, B., Zhang, Z., Jacob, D.E., Gillikin, D., Tütken, T., Garbe-Schönberg, D., McConaughey, T., Soldati, A., 2010. Effect
310 of organic matrices on the determination of the trace element chemistry (mg, sr, mg/ca, sr/ca) of aragonitic bivalve shells
311 (*arctica islandica*)—comparison of ICP-OES and LA-ICP-MS data. *Geochemical Journal* 44, 23–37. doi:[10.2343/GEOCHEMJ.1.0045](https://doi.org/10.2343/GEOCHEMJ.1.0045).
- 312 Shackleton, N.J., 1973. Oxygen isotope analysis as a means of determining season of occupation of prehistoric midden sites.
313 *Archaeometry* 15, 133–141. doi:[10.1111/j.1475-4754.1973.tb00082.x](https://doi.org/10.1111/j.1475-4754.1973.tb00082.x).
- 314 Surge, D., Barrett, J.H., 2012. Marine climatic seasonality during medieval times (10th to 12th centuries) based on isotopic
315 records in viking age shells from orkney, scotland. *Palaeogeogr. Palaeoclimatol. Palaeoecol.* 350–352, 236–246. doi:[10.1016/j.palaeo.2012.07.003](https://doi.org/10.1016/j.palaeo.2012.07.003).
- 316 Surge, D., Lohmann, K.C., 2008. Evaluating mg/ca ratios as a temperature proxy in the estuarine oyster, *Crassostrea virginica*:
317 Mg/ca RATIOS IN OYSTER SHELLS. *J. Geophys. Res.* 113, G02001. doi:[10.1029/2007jg000623](https://doi.org/10.1029/2007jg000623).
- 318 Vihtakari, M., Ambrose, Jr, W.G., Renaud, P.E., Locke, V., W.L., Carroll, M.L., Berge, J., Clarke, L.J., Cottier, F., Hop,
319 H., 2017. A key to the past? element ratios as environmental proxies in two arctic bivalves. *Palaeogeogr. Palaeoclimatol.*
320 *Palaeoecol.* 465, 316–332. doi:[10.1016/j.palaeo.2016.10.020](https://doi.org/10.1016/j.palaeo.2016.10.020).
- 321 Villagran, X.S., Balbo, A.L., Madella, M., Vila, A., Estevez, J., 2011. Stratigraphic and spatial variability in shell middens:
322 microfacies identification at the ethnohistoric site tunel VII (tierra del fuego, argentina). *Archaeol. Anthropol. Sci.* 3, 357–378.
323 doi:[10.1007/s12520-011-0074-z](https://doi.org/10.1007/s12520-011-0074-z).
- 324 Wanamaker, Jr, A.D., Kreutz, K.J., Wilson, T., Borns, Jr, H.W., Introne, D.S., Feindel, S., 2008. Experimentally determined
325 mg/ca and sr/ca ratios in juvenile bivalve calcite for *mytilus edulis*: implications for paleotemperature reconstructions.
326 *Geo-Mar. Lett.* 28, 359–368. doi:[10.1007/s00367-008-0112-8](https://doi.org/10.1007/s00367-008-0112-8).
- 327 Wang, T., Surge, D., Mithen, S., 2012. Seasonal temperature variability of the neoglacial (3300–2500BP) and roman warm
328 period (2500–1600BP) reconstructed from oxygen isotope ratios of limpet shells (*patella vulgata*), northwest scotland. *Palaeo-*

- 335 geogr. Palaeoclimatol. Palaeoecol. 317-318, 104–113. doi:[10.1016/j.palaeo.2011.12.016](https://doi.org/10.1016/j.palaeo.2011.12.016).
- 336 Zangrando, A.F.J., Ponce, J.F., Martinoli, M.P., Montes, A., Piana, E., Vanella, F., 2016. Palaeogeographic changes drove
337 prehistoric fishing practices in the cambaceres bay (tierra del fuego, argentina) during the middle and late holocene. Environ.
338 Archaeol. 21, 182–192. doi:[10.1080/14614103.2015.1130888](https://doi.org/10.1080/14614103.2015.1130888).
- 339 Álvarez, M., Briz Godino, I., Balbo, A., Madella, M., 2011. Shell middens as archives of past environments, human dispersal
340 and specialized resource management. Quat. Int. 239, 1–7. doi:[10.1016/j.quaint.2010.10.025](https://doi.org/10.1016/j.quaint.2010.10.025).